

On Rainbows from Inhomogeneous Transparent Spheres: A Ray-Theoretic Approach

John A. Adam & Philip Laven

John A. Adam, Department of Mathematics & Statistics at Old Dominion University, Norfolk, Virginia 23529

Philip Laven, Chemin de l'Avanchet 20, CH-1216 Cointrin, Geneva, Switzerland

A ray-theoretic account of the passage of light through a radially inhomogeneous transparent sphere has been used to establish the existence of *multiple* primary rainbows for some refractive index profiles. The existence of such additional bows is a consequence of a sufficiently attractive potential in the interior of the drop, i.e. the refractive index gradient should be sufficiently negative there. Profiles for which this gradient is monotonically increasing do not result in this phenomenon, but non-monotone profiles can do so, depending on the form of n . Sufficiently oscillatory profiles can lead to apparently singular behavior in the deviation angle (within the geometrical optics approximation) as well as multiple rainbows. These results may be of value in the field of rainbow refractometry.

OCIS codes: 080.2710

Introduction: Rays in radially inhomogeneous media

Using elementary differential geometry, it may be shown that if $\boldsymbol{\eta}$ is the radius vector of a point on a ray, and \mathbf{s} is the tangent vector at that point, and $n(\eta)$ is the refractive index, then in terms of $\boldsymbol{\eta}$ and $\eta = |\boldsymbol{\eta}|$,

$$\boldsymbol{\eta} \times n(\eta) \mathbf{s} = \text{constant}. \quad (1)$$

This result, known as Bouguer's formula¹, implies that all the ray paths are plane curves, in a plane through the origin, and that along each ray

$$n(\eta) \eta \sin \phi = \text{constant} = K. \quad (2)$$

where ϕ is the angle between the vector $\boldsymbol{\eta}$ and the tangent to the ray at that point. In a spherically symmetric medium, elementary geometry (in terms of the polar coordinates of a plane) indicates that

$$\sin \phi = \frac{\eta(\theta)}{\sqrt{\eta^2(\theta) + (d\eta/d\theta)^2}}. \quad (3)$$

Equations (2) and (3) imply that

$$\frac{d\eta}{d\theta} = \pm \frac{\eta}{K} \sqrt{\eta^2 n^2(\eta) - K^2},$$

whence the governing equation for ray paths in spherically symmetric media is

$$\theta - \theta_0 = \pm K \int_R^\xi \frac{d\eta}{\eta \sqrt{\eta^2 n^2(\eta) - K^2}}. \quad (4)$$

In this integral the upper limit of the radial variable η is the dummy variable ξ , where $0 \leq \xi \leq R$, R being the radius of the sphere. The initial angle θ_0 corresponds to the value of θ when $\xi = R$, namely at the point of entry of the ray into the sphere. To derive an expression for the total deviation $D(i)$ undergone by a ray after two refractions and one reflection, initially incident at angle i , that is a generalization of the primary rainbow ray "path", the procedure is as follows. First consider $n'(\eta) < 0$ as in Fig. 1(a). By symmetry, $\text{arc}PQ = \text{arc}QS = \text{arc}ST = \text{arc}TV$. As the ray moves along the path PQ from P to Q , θ is increasing while ξ is decreasing, so $d\theta/d\xi < 0$. Equivalently, if s is the arc length along the ray, $d\theta/ds > 0$ and $d\xi/ds < 0$ on this portion of the path. The $\theta = 0$ axis is oriented parallel to the incoming ray, so $\theta_0 = i$, the angle of incidence. The total deviation along the path $PQSTV$ in this case is

$$D(i) = 2i + \pi - 4r(i) + \Theta, \quad (5)$$

where Θ is the deviation due to the non-zero curvature of the ray path. Thus Θ represents the excess deviation over the constant refractive index case, and by symmetry it is four times the excess deviation from P to Q . The exact shape of the path obviously depends on the choice for $n(\eta)$. It will be assumed that $n(\eta)$ is continuous in the interval $(0, R)$. To elucidate the functional form of Θ , consider the point Q on the path, corresponding to the stationary angle $\bar{\theta}$ in the diagram, i.e. where

$$\left. \frac{d\xi}{d\theta} \right|_{\bar{\theta}} = 0. \quad (6)$$

Recall from equation (4) that

$$\frac{d\theta}{d\xi} = -\frac{K}{\xi\sqrt{\xi^2 n^2(\xi) - K^2}}.$$

The choice of $-K$, where $K > 0$ has been made because $\theta'(\xi) < 0$ on the portion PQ of the arc. Thus condition (6) occurs when (i) $\xi = 0$, and (ii) more interestingly, when $\xi^2 n^2(\xi) = K^2$. This provides a natural definition of the *turning point* $\bar{\xi}$, where $\bar{\xi} \equiv \xi(\bar{\theta})$; on arc PQ (or any equivalent arc) this mapping is invertible for a given sign of K , so we also have a more useful form $\bar{\theta} \equiv \theta(\bar{\xi})$. As can be seen from Fig. 1(a), this is the point at which a ray propagating into the droplet is refracted away from its closest point of entry to the center (in the case of constant n , the interior ray path is straight of course, but $\bar{\xi}$ still defines the point of closest approach to the origin).

It is convenient to employ a dimensionless version of some of the above equations in what follows, scaling radial distances within the sphere by the radius R . Let $\lambda = \eta/R$, $\bar{\lambda} = \bar{\xi}/R$, where $0 \leq \bar{\lambda} \leq \lambda \leq 1$, and $\bar{K} = K/R$. At the point of entry P , the angle $\phi = r(i)$, the angle of refraction (see equation (2)). The value of \bar{K} determines the subsequent path of any incident ray. Since $n(\lambda)$ is discontinuous at $\lambda = 1$, it follows that

$$\bar{K}(i) = \lim_{\lambda \rightarrow 1^-} [\lambda n(\lambda)] \sin r(i) = \lim_{\lambda \rightarrow 1^-} \lambda \sin i = \sin i, \text{ but when } \lambda = \bar{\lambda},$$

$$\bar{K} = \bar{\lambda} n(\bar{\lambda}) \sin[\phi(\bar{\lambda})] = \bar{\lambda} n(\bar{\lambda}) \sin[\pi/2] = \bar{\lambda} n(\bar{\lambda}),$$

so that in principle $\bar{\lambda}$ may be determined for a given refractive index profile from the result

$$\bar{K} = \bar{\lambda} n(\bar{\lambda}) = \sin i, \quad (7)$$

Notice also that in general the solution $\bar{\lambda}$ will not be unique, but in practice it should be straightforward to identify the physically significant one. From equation (4) for $\theta = \bar{\theta}$, in dimensionless terms,

$$\bar{\theta} - i = -\bar{K} \int_1^{\bar{\lambda}} \frac{d\eta}{\eta \sqrt{\eta^2 n^2(\eta) - K^2}} = \bar{K} \int_{\bar{\lambda}}^1 \frac{d\lambda}{\lambda \sqrt{\lambda^2 \bar{n}^2(\lambda) - \bar{K}^2}} \equiv \bar{K} I(\bar{\lambda}, i), \quad (8)$$

where $\bar{n}(\lambda) = n(\eta)$. This expression is related to $D(i)$ using Fig. 1(b). For any convex quadrilateral

$$\beta = -\pi + 2(r + \bar{\theta} - i), \quad (9)$$

(and so $\beta = 0$ when $n = \text{constant}$.) For the total path $PQSTV$, $\Theta = 2\beta$, from which it follows that for $n'(r) > 0$ the total deviation for a primary bow is, from (5)

$$D(i) = 2i - \pi + 4\bar{K} \int_{\bar{\lambda}}^1 \frac{d\lambda}{\lambda \sqrt{\lambda^2 \bar{n}^2(\lambda) - \bar{K}^2}}. \quad (10)$$

As shown in the appendix, this result reduces to the known result for $n = \text{constant}$. Clearly, the integral in (10) is improper at the lower limit. This corresponds of course to the definition of $\bar{\lambda}$, the value of λ at which $\lambda'(\theta) = 0$; in practice, the integral exists for reasonable choices of $\bar{n}(\lambda)$. In the case for which $\bar{n}'(\lambda) < 0$, the curvature is away from the center, i.e. in the clockwise sense this time, so equation (5) still applies, but now β is defined as

$$\beta = \pi - 2(r + \bar{\theta} - i), \quad (9')$$

A specific refractive index profile

A specific monotonically decreasing profile for $\bar{n}(\lambda)$ will be chosen that has several advantages, one being reasonable analytic tractability (in the perturbation analysis to follow) and which readily illustrates the “double rainbow” phenomenon. The choice below for $\bar{n}(\lambda)$ was made because the gradient $\bar{n}'(\lambda)$ is *not* constant, thereby allowing for the possibility of subtle features that may not be present in a linear profile. While it may be argued that a linear profile is simpler to investigate, this is not in fact the case: the latter contains a quartic term in the radicand of the integral, and results in elliptic integrals that, analytically at least, provide little insight into the physics of the problem; furthermore, for this profile $\bar{\lambda}$ is not unique. The equation for $\bar{\lambda}$ in this case is admittedly only a quadratic, and it is physically obvious which root to take, but this lends a minor but additional complication to a less general and yet more complex case. Furthermore, since any smooth profile can be reasonably approximated by a linear Taylor polynomial for a sufficiently “small” inhomogeneity, the choice of $\bar{n}(\lambda)$ below contains the linear profile as a special case. This idea is used in the perturbation analysis below: although $\bar{\lambda}$ is known exactly for this refractive index profile it is nonlinear in “ $\sin i$ ” and a linearization of $\bar{\lambda}$ about its value for n_0 for a homogeneous sphere is very useful in evaluating the integrals below. The choice for $\bar{n}(\lambda)$ is subject to the “boundary conditions” $\bar{n}(0) \equiv n_0$ and $\bar{n}(1) \equiv n_1$, where $n_0 > n_1$. This determines the parameters $a(= (n_0 - n_1)/n_0 n_1)$ and $b(= n_0^{-1})$ in the chosen profile

$$\bar{n}(\lambda) = (a\lambda + b)^{-1} \equiv \frac{n_0 n_1}{(n_0 - n_1)\lambda + n_1}. \quad (11)$$

The expression for the minimum impact parameter $\bar{\lambda}(i)$ is found by solving equation (7) to give

$$\bar{\lambda} = \frac{n_1 \sin i}{n_0 n_1 - (n_0 - n_1) \sin i}. \quad (12)$$

Because the numerator is increasing and the denominator is decreasing with i , it follows from equation (12) that $\bar{\lambda}$ is an increasing function of i on $(0, \pi/2)$. Now the integral in equation (10) reduces to

$$I(\bar{\lambda}, i) = \int_{\bar{\lambda}}^1 \frac{(a\lambda + b)d\lambda}{\lambda \sqrt{\lambda^2 - \bar{K}^2} (a\lambda + b)^2} \equiv aI_A + bI_B, \quad (13)$$

$$\text{where } I_A = \int_{\bar{\lambda}}^1 \frac{d\lambda}{\sqrt{C\lambda^2 + B\lambda + A}}, \quad (14)$$

$$I_B = \int_{\bar{\lambda}}^1 \frac{d\lambda}{\lambda \sqrt{C\lambda^2 + B\lambda + A}}, \quad (15)$$

$$\text{and } C \equiv 1 - a^2 \bar{K}^2 = \left(1 - \left[\frac{n_0 - n_1}{n_0 n_1} \right]^2 \sin^2 i \right) > 0,$$

$$B \equiv -2ab\bar{K}^2 = -2 \left[\frac{n_0 - n_1}{n_0 n_1} \right] \sin^2 i, \quad A \equiv -b^2 \bar{K}^2.$$

The positivity of C follows from the fact that $n_0 - n_1 < n_0 n_1$ always for $n_1 \geq 1$. The above integrals are standard forms, so equation (13) can be recast into $I(1, i) - I(\bar{\lambda}, i)$, where

$$I(\lambda, i) = \frac{a \ln \left(2\sqrt{C(C\lambda^2 + B\lambda + A)} + 2C\lambda + B \right)}{\sqrt{C}} + \frac{b}{\sqrt{-A}} \arcsin \frac{2A + B\lambda}{\lambda \sqrt{B^2 - 4AC}}. \quad (16)$$

Perturbation analysis

To illustrate the effects of slight non-homogeneity in $n(\eta)$ the profile parameter a will be considered small and equal to ε , the expansion parameter in what follows. [This forces $n_1 = 5(5\varepsilon + 3)^{-1}$, but this presents no difficulty because $n_1 \geq 1$ provided $\varepsilon \leq 0.4$.] The integral (14) will be expanded in powers of ε and inserted into expression (10) for $D(i)$, retaining only terms up to $O(\varepsilon)$ in both individual expansions and the final result. Interestingly, terms of $O(\varepsilon^{1/2})$, $O(\varepsilon)$ and $O(\varepsilon^{3/2})$ arise, but the terms $O(\varepsilon^{1/2})$ vanish identically. Up to $O(\varepsilon)$, expression (14) is

$$I(\bar{\lambda}, i) = \int_{\bar{\lambda}}^1 \left(a + \frac{b}{\lambda} \right) \left[\frac{1}{\sqrt{\lambda^2 - \bar{K}^2 b^2}} + \frac{2\varepsilon \lambda b \bar{K}^2}{(\lambda^2 - \bar{K}^2 b^2)^{3/2}} \right] d\lambda \quad (17)$$

$$\equiv I_1 + I_2 + I_3 + I_4,$$

where the integrals I_k , $k = 1, 2, 3, 4$ for now will remain indefinite. They are

$$I_1 = a \int \frac{d\lambda}{\sqrt{\lambda^2 - \bar{K}^2 b^2}} = a \ln \left(\lambda + \sqrt{\lambda^2 - \bar{K}^2 b^2} \right);$$

$$I_2 = b \int \frac{d\lambda}{\lambda \sqrt{\lambda^2 - \bar{K}^2 b^2}} = -\frac{1}{\bar{K}} \arcsin \left(\frac{\bar{K} b}{\lambda} \right);$$

$$I_3 = 2\varepsilon a b \bar{K}^2 \int \frac{\lambda d\lambda}{(\lambda^2 - \bar{K}^2 b^2)^{3/2}} = -\frac{2\varepsilon a b \bar{K}^2}{\sqrt{\lambda^2 - \bar{K}^2 b^2}};$$

$$I_4 = 2\varepsilon b^2 \bar{K}^2 \int \frac{d\lambda}{(\lambda^2 - \bar{K}^2 b^2)^{3/2}} = -\frac{2\varepsilon \lambda}{\sqrt{\lambda^2 - \bar{K}^2 b^2}}.$$

Also condition (7) implies that

$$\bar{\lambda} = (\varepsilon \bar{\lambda} + b) \sin i, \text{ i.e. } \bar{\lambda} = b \sin i (1 + \varepsilon \sin i) + O(\varepsilon^2). \quad (18)$$

The expression $(\lambda^2 - \bar{K}^2 b^2)^{1/2}$ appears in various ways in the above integrals. It is readily verified that $(\lambda^2 - \bar{K}^2 b^2)^{1/2} = \sqrt{2} b \varepsilon^{1/2} \sin^{3/2} i + O(\varepsilon^{3/2})$. After some algebra the *definite* integrals are as follows:

$$\begin{aligned} [I_1]_{\bar{\lambda}}^1 &= \varepsilon \ln \left(\frac{1 + (\lambda^2 - \bar{K}^2 b^2)^{1/2}}{b \sin i} \right) + O(\varepsilon^{3/2}); \\ [I_2]_{\bar{\lambda}}^1 &= -\frac{1}{K} \left[\arcsin(\bar{K}b) - \frac{\pi}{2} + (2\varepsilon \sin i)^{1/2} \right] + O(\varepsilon^{3/2}); \\ [I_3]_{\bar{\lambda}}^1 &= O(\varepsilon^{3/2}); \\ [I_4]_{\bar{\lambda}}^1 &= \left(\frac{2\varepsilon}{\sin i} \right)^{1/2} - \frac{2\varepsilon}{(1 - \bar{K}^2 b^2)^{1/2}} + O(\varepsilon^{3/2}). \end{aligned}$$

These results are then substituted into equation (10), resulting in (to $O(\varepsilon)$)

$$\begin{aligned}
D(i) &= 2i - \pi + \\
&4\bar{K} \left\{ \begin{aligned} &\varepsilon \ln \left(\frac{1 + (1 - \bar{K}^2 b^2)^{1/2}}{b \sin i} \right) - \frac{1}{\bar{K}} \left[\arcsin(\bar{K}b) - \frac{\pi}{2} + (2\varepsilon \sin i)^{1/2} \right] + \\ &\left(\frac{2\varepsilon}{\sin i} \right)^{1/2} - \frac{2\varepsilon}{(1 - \bar{K}^2 b^2)^{1/2}} \end{aligned} \right\} + O(\varepsilon^{3/2}) \\
&\approx 2i + \pi - 4 \arcsin(\bar{K}b) + 4\varepsilon \bar{K} \left\{ \ln \left(\frac{1 + (1 - \bar{K}^2 b^2)^{1/2}}{b \sin i} \right) - \frac{2}{(1 - \bar{K}^2 b^2)^{1/2}} \right\} \\
&= 2i + \pi - 4 \arcsin(b \sin i) + 4\varepsilon \sin i \left\{ \ln \left(\frac{1 + (1 - b^2 \sin^2 i)^{1/2}}{b \sin i} \right) - \frac{2}{(1 - b^2 \sin^2 i)^{1/2}} \right\}. \tag{18a} \\
&\equiv D_h(i) + \varepsilon F(i),
\end{aligned}$$

$$\text{where } F(i) = 4 \sin i \left\{ \ln \left(\frac{1 + (1 - b^2 \sin^2 i)^{1/2}}{b \sin i} \right) - \frac{2}{(1 - b^2 \sin^2 i)^{1/2}} \right\},$$

and $D_h(i)$ is the deviation for the homogeneous sphere (this follows because $b = n_0^{-1}$), and $\varepsilon F(i)$ is the additional deviation, to $O(\varepsilon)$, due to the non-homogeneous refractive index. In order to determine where an extremum of $D(i)$ occurs (if it does) relative to the homogeneous case (occurring at $i = i_c$ say), let us use first degree Taylor polynomials in the following manner: clearly, since from equation 18a, it follows that $D'(i) = D_h'(i) + \varepsilon F'(i)$. Near $i = i_c$, $i = i_c + \delta$, say ($|\delta| \ll i_c$), $F(i) \approx F(i_c) + \delta F'(i_c)$. Then $D'(i) \approx 0 + \delta D_h''(i_c) + \varepsilon F'(i_c)$ to first order in small quantities δ, ε . Since a necessary condition for the existence of extrema in $D(i)$ is $D'(i) = 0$, it follows that

$$\delta D_h''(i_c) + \varepsilon [F'(i_c) + \delta F''(i_c)] \approx 0, \text{ or}$$

$$\delta \approx -\frac{\varepsilon F'(i_c)}{D_h''(i_c) + \varepsilon F''(i_c)} = -\frac{\varepsilon F'(i_c)}{D_h''(i_c)} + O(\varepsilon^2). \quad (19)$$

Elementary ray theory shows that $D_h''(i_c) > 0$, and $F'(i_c) < 0$ for $n_0 = 5/3$ (as is readily verified from Fig. 2), it follows that $\delta > 0$ in the vicinity of i_c , i.e. the extremum occurs at slightly higher values of i than compared with the homogeneous case. Indeed, from the general shape of $F(i)$ in Fig. 2 it may be seen that $F(i) > 0$ for $i \in (0, \mu)$, where $\mu \approx 0.429$ for $n_0 = 5/3$ and $F(i) < 0$ for $i \in (\mu, \pi/2]$. This is consistent with the fact that compared with the homogeneous sphere, according to Fig. 3, there is now a maximum of $D(i)$ in $(0, \mu)$ and the minimum of $D(i)$ in $(\mu, \pi/2]$ is lower, i.e. $D(i_{\min}) < D_h(i_c)$. The reason for this is that initially, $F(i)$ increases faster than $D_h(i)$ decreases, so $D(i)$ also increases, decreasing shortly thereafter (according to Fig. 3, at $i \approx 16.3^\circ$ OK). In fig. 2, the solid curve ($F(i)$) is drawn for $n_0 = 5/3$ while the dashed curve ($FI(i)$) is for $n_0 = 2.5$. In fig. 3, $\varepsilon = 0.25$ and $n_0 = 5/3$, but even for this relatively large “inhomogeneity” the agreement between the exact “TotD(i)” and the linear approximation given by equation (18) is quite close. The disparity between these two graphs shrinks (as one would expect) as ε tends to zero.

Note that the above profile for $\bar{n}(\lambda)$ was chosen for analytic convenience; it also has the advantage that a unique value of $\bar{\lambda}$ could be specified for numerical studies. In general this is not the case. However, as noted earlier, to the extent that any profile can be approximated (sometimes quite accurately) by a linear Taylor polynomial, this result is general in that it holds for any small functional deviation from a constant profile n_0 .

Power law profiles for $n(r)$

Earlier work by Brockman and Alexopoulos³ considered ray optics for particles with refractive indices in the form of a power law; in dimensional notation $n(r) = n(R)(r/R)^m$. This functional form allows for two very unphysical situations: $n(0) = 0$ when $m > 0$ and $n(0) \rightarrow \infty$ as $r \rightarrow 0$ when $m < 0$. If however, a constant index sphere of radius $a < R$ were smoothly matched to this type of profile for $a < r < R$, then such a composite profile might prove useful. Even without modification it represents two extreme cases of very weak and very strong central refraction respectively.

For the simple power law index, the expression (10) for $D(i)$ is reducible to a generalization of that for constant n . In terms of the dimensionless variable λ , $n(\lambda) = n(1)\lambda^m \equiv n_1\lambda^m$, where $n_1 > 1$. As shown in the appendix, for q internal reflections within the drop,

$$D(i) = 2i - \pi + \frac{2(q+1)}{m+1} \left(\frac{\pi}{2} - r \right) = 2i + \left(\frac{q-m}{1+m} \right) \pi - \frac{2(q+1)r}{m+1}, \quad (20)$$

where $m > -1$. [Brockman *et al.* call $D(i)$ the total bend angle, but they use the letter p to denote the number of internal reflections. This can be confusing, because in the optics literature $p \geq 1$ is usually reserved for the order of Debye series contributions, so the number of internal reflections is given by $p-1$. Thus $p = 0$ corresponds to external reflection plus diffraction, $p = 1$ corresponds to direct transmission through the sphere, $p = 2$ corresponds to 1 internal reflection (primary rainbow), $p = 3$ corresponds to 2 internal reflections (secondary rainbow) and so on.

Proceeding in the usual manner to locate an extremum of $D(i)$ we find that the critical angle of incidence, i_c , for an extremum (here a minimum) of $D(i)$ is given by

$$i_c = \arccos \left\{ (m+1) \sqrt{\frac{n_1^2 - 1}{(q+1)^2 - (m+1)^2}} \right\} \quad (21)$$

Clearly, this expression places restrictions on q in terms of m (or vice versa). If for some real number s we define $[s]$ to mean the smallest non-negative integer larger than s , then the requirement that the argument of the inverse cosine is in the interval $[0,1]$ leads to the dual conditions (for $n_1 \geq 1$ and $m > -1$)

$$q \geq [m] \text{ and } q \geq [(m+1)n_1 - 1]. \quad (22)$$

Examination of the straight lines $q_1 = m$ and $q_2 = (m+1)n_1 - 1$ shows that $q_2 > q_1$ for $m > -1$.

When the constraints on m are expressed in terms of q the $[.]$ notation is unnecessary. Indeed

$$m \leq m_1 = q \text{ and } m \leq m_2 = \frac{q+1}{n_1} - 1. \quad (23)$$

These lines are the inverses of those in equation (22), and so $m \leq m_2$. Let us examine the particular case of $q = 0$: only internal refraction (or direct transmission) occurs. It is still possible for a “zeroth-order” rainbow to occur provided $m \leq n_1^{-1} - 1$, so for $n_1 = 4/3$, this means $m \leq -0.25$., i.e. the refractive index must be sufficiently “attractive” near the center of the sphere. For $q = 1$ even a mildly “repulsive” refractive index will suffice to induce a rainbow for this value of n_1 provided $m < 0.5$.

The existence of multiple rainbows of a given order

The model of Brockman et al. does not allow for the possibility of more than one rainbow of a given order since $D'(i)$ from equation (20) possesses the unique zero i_c . Some insights about

when this phenomenon may occur can be gained by examining the quantity $\rho(\lambda) = \lambda \bar{n}(\lambda)$ ($= \bar{K} = \sin i$) in equation (10). The turning point $\bar{\lambda}$ for a ray with a given angle of incidence i is given implicitly by the relation $\rho(\bar{\lambda}) = \sin i$. Fig. 4 shows two refractive index profiles: $\rho_1(\lambda) = \lambda \bar{n}_1(\lambda) = \lambda[5 - 4(\lambda - 0.5)^2]/3$ and $\rho_2(\lambda) = \lambda \bar{n}_2(\lambda) = 4\lambda[1 + (\lambda - 0.5)^2]/3$. The first corresponds to the refractive index increasing from $4/3$ at $\lambda = 0$ to a maximum of $5/3$ at $\lambda = 0.5$ and then decreasing back to $4/3$ at the drop surface, $\lambda = 1$. The second profile corresponds to the refractive index *decreasing* from $5/3$ at $\lambda = 0$ to a minimum of $4/3$ at $\lambda = 0.5$ and then increasing back to $5/3$ at the drop surface, $\lambda = 1$. The $D(i)$ graphs corresponding to these two symmetric refractive index profiles exhibit interesting differences (see Fig. 5) for \bar{n}_1 there is a single minimum near $i = 13.8^\circ$ of arc, whereas for \bar{n}_2 there is a maximum near $i = 8.0^\circ$ and a minimum near $i = 65.3^\circ$ – a double primary rainbow! Clearly the presence of an attractive index profile n_2 in the central region is the physical reason for this. However, despite the different concavities of both the \bar{n} and the ρ profiles, there is nothing distinctive in these graphs to indicate this contrasting behavior. Perhaps this is not surprising given that it is a weighted integral of the reciprocal square root of $\rho^2 - \sin^2 i$ that is contributing to $D(i)$. It is worth noting that similar results occur for the linear profiles $n = (4 + \lambda)/3$ (minimum only) and $n = (5 - \lambda)/3$ (maximum and minimum).

Nevertheless, further insight may be gained from the more complicated profile $\bar{n}(\lambda) = [5 + \sin(6\pi\lambda)]/3$. This and the corresponding $\rho(\lambda)$ graph are shown in Fig. 6. Recall that the turning point $\bar{\lambda}$ is defined by the equation $\rho(\bar{\lambda}) = \sin i$, so the vertical axis is synonymous with $\sin i$ as far as $\bar{\lambda}$ is concerned, and therefore it is only of interest to consider $0 \leq \rho \leq 1$. Consider an incoming ray with angle of incidence i increasing from zero to 90° . The axial ray

passes through the center and for $q = 1$ (of interest here), $\bar{\lambda}$ is obviously zero. As i increases, so too does $\bar{\lambda}$, changing slowly as a function of i at first, and more rapidly later, because the derivative of ρ as drawn is decreasing until the point of inflection is reached. (For portions of the graph in which $\rho'(\bar{\lambda}) > 0$, this effect is reversed, $\bar{\lambda}(i)$ increases rapidly at first and then slows.) However, at the value of $\sin i$ corresponding to the relative minimum of $\rho(\bar{\lambda})$, $\bar{\lambda}$ jumps discontinuously on this graph from approximately 0.39 to about 0.57 and then climbs to about 0.64. If instead of starting at i equal to zero we had reversed the process, starting with a tangentially incident ray ($\sin i = 1$), the “track” of $\bar{\lambda}$ is reversible. At the relative minimum of $\rho(\bar{\lambda})$, this being the coalescence of two turning points (the “inner” one being inaccessible to an incoming ray), we might expect some correspondingly aberrant behavior in $D(i)$, and this does indeed occur (see Fig. 7). The “spiked” behavior evident in this figure. is therefore associated with the discontinuity in the turning point $\bar{\lambda}(i)$.

Another feature is noteworthy. It appears that for at least monotonically decreasing $n(r)$ profiles, the quantity

$$L(i) = \bar{K} \int_{\bar{\lambda}}^1 \frac{d\lambda}{\lambda \sqrt{\lambda^2 n^2(\lambda) - \bar{K}^2}} \quad (24)$$

possesses a point of inflection, while for monotonically increasing profiles it does not, exhibiting only a graph with upward concavity. Furthermore, it is apparent from Fig. 8 (drawn for a linearly decreasing refractive index profile) that the derivative $L'(i)$ is negative in the interval of interest. These are obviously necessary conditions for the existence of double extrema in the graph of $D(i)$, since the remaining terms are linear in i . This feature is also present for the parabolic

profile $n(r) = 4[1 + (r - 0.5)^2]/3$, so it appears that the double bow exists provided the profile is sufficiently attractive in the deep interior of the drop.

Nevertheless, these general criteria on $L(i)$ are still insufficient to translate into conditions on $n(r)$. In the graphs below for $n(\lambda) = (5 - \lambda)/3$ (Fig. 8), $D(i)$ is the total deviation (10) and $Dl(i)$ is just the linear part of $D(i)$, namely $Dl(i) = 2i$.

Conclusion

A ray-theoretic account of the passage of light through a radially inhomogeneous transparent sphere has been used to establish the existence of *multiple* (≥ 2) primary rainbows (and in principle, higher-order bows) for some refractive index profiles. The existence of such additional bows is a consequence of a sufficiently “attractive potential” in the interior of the drop, i.e. the refractive index gradient should be sufficiently negative there. Profiles for which this gradient is monotonically increasing do not result in this phenomenon, but non-monotone profiles can do so, depending on the form of n . Indeed, sufficiently oscillatory profiles can lead to apparently singular behavior in the deviation angle (within the geometrical optics approximation) as well as multiple rainbows.

These results may be of value in the field of rainbow refractometry and thermometry, which are optical techniques used to measure the refractive index (and hence temperature) of transparent particles (including fuel droplets), and the cross-sectional shape of dielectric cylinders⁵⁻²². These techniques can be used to determine very small spatial and time-varying changes in refractive index, and are valuable for analysis of the combustion of liquid hydrocarbons, the injection of sprays in high-pressure environments, as well as spraying/drying techniques employed in the food, agricultural and pharmaceutical industries¹³. Gradients of

refractive index can be caused when droplets undergo simultaneous heating and evaporation in a combustion chamber, and will be primarily radial if internal convection can be neglected compared with thermal conduction¹⁴. Similar refractometry studies have been carried out to determine the refractive indices and radii of unclad optical fibers²³⁻²⁵. While much of the work referenced above is based on geometrical optics, some utilize the more sophisticated Airy and/or Lorenz-Mie theories, explicitly or implicitly^{15,17-20}, and most recently, generalizations of the Airy theory in combination with geometrical optics have been carried out^{26,27}. The present study provides a basis for investigation of more complex radial gradients in refractive index than has hitherto been the case.

Appendix

(i) constant n

For the case of constant $n = N$, it is seen from a straightforward modification of Fig. 1b' that $\bar{\xi} = R \sin r = (R \sin i) / N = K / N \equiv a$, so that

$$\begin{aligned} \int_{\bar{\xi}}^R \frac{d\eta}{\eta \sqrt{\eta^2 N^2(\eta) - K^2}} &= \frac{1}{N} \int_{\bar{\xi}}^R \frac{d\eta}{\eta \sqrt{\eta^2 - a^2}} = \frac{1}{aN} \left(\operatorname{arcsec} \frac{R}{a} - \operatorname{arcsec} \frac{\bar{\xi}}{a} \right) \\ &= \frac{1}{K} \left(\operatorname{arcsec}(\csc r) - \operatorname{arcsec} 1 \right) = \frac{1}{K} \left(\frac{\pi}{2} - r \right) > 0. \end{aligned}$$

Therefore

$$D(i) = 2i - \pi + 4K \left(\frac{\pi/2 - r}{K} \right) = 2i + \pi - 4r,$$

as is required.

(ii) Derivation of equation (20)

Starting with equation (10), let $n(\lambda) = n_1 \lambda^m$, $n_1 > 1$. Then the integral in equation (10) is

$$\int_{\bar{\lambda}}^1 \frac{d\lambda}{\lambda \sqrt{n_1^2 \lambda^{2m+2} - \bar{K}^2}} = \frac{1}{m+1} \int_{\bar{y}}^{n_1} \frac{dy}{y \sqrt{y^2 - \bar{K}^2}}$$

in terms of $y = n_1 \lambda^{m+1}$ and $\bar{y} = n_1 \bar{\lambda}^{m+1}$, where $m+1 > 0$. This new integral is the same standard form as in part (i) above, and so equals

$$\frac{1}{(m+1)\bar{K}} \left[\arccos \left(\frac{n_1 \lambda^{m+1}}{\bar{K}} \right) \right]_{\bar{\lambda}}^1 = \frac{1}{m+1} \left(\frac{\pi}{2} - r \right).$$

This is half the internal ‘‘bend angle’’ for direct transmission, and the bend angle is multiplied by q ($q \geq 1$) for q internal reflections, resulting in

$$D(i) = 2i - \pi + \frac{2(q+1)}{m+1} \left(\frac{\pi}{2} - r \right),$$

this being is the first form of equation (20).

(iii) Alternative formulation

Returning to the case of a general profile $\bar{n}(\lambda)$, equation (10) for $D(i)$ can be recast as follows:

define a new dependent variable $y(\lambda) \equiv \lambda \bar{n}(\lambda)$. In terms of differentials, $d\lambda = (dy - \lambda d\bar{n})/\bar{n}$

and so the integral in (10) can be rewritten as the sum of two others (note the order of the limits in the second integral), i.e.

$$\int_{\bar{\lambda}}^1 \frac{d\lambda}{\lambda \sqrt{\lambda^2 \bar{n}^2(\lambda) - \bar{K}^2}} = \int_{\bar{K}}^{n_1} \frac{dy}{y \sqrt{y^2 - \bar{K}^2}} + \int_{n_1}^{n(\bar{\lambda})} \frac{d\bar{n}}{\bar{n} \sqrt{y^2(\bar{n}) - \bar{K}^2}} \equiv I_\alpha + I_\beta.$$

Now

$$\int_{\bar{K}}^{n_1} \frac{dy}{y \sqrt{y^2 - \bar{K}^2}} = \frac{1}{\bar{K}} \left[\text{arc sec} \left(\frac{y}{\bar{K}} \right) \right]_{\bar{K}}^{n_1} = \frac{1}{\bar{K}} \text{arc sec} \left(\frac{n_1}{\sin i} \right) = \frac{1}{\bar{K}} \left(\frac{\pi}{2} - r \right),$$

so the contribution to $D(i)$ from the first three terms, $2i - \pi + 4\bar{K}I_\alpha = 2i + \pi - 4r$, is just the deviation for a primary bow produced by a sphere of constant refractive index n_1 . Thus the second integral represents the additional contribution from the inhomogeneity of the sphere. In this respect it is a generalization of perturbation result (18), with the difference that the homogeneous part refers to a sphere with refractive index n_r as opposed to n_0 . The second integral, I_β , is more problematical because it requires the quantity $y(\lambda) = \lambda \bar{n}(\lambda)$ to be expressed in terms of \bar{n} . This alternative formulation may prove useful for subsequent theoretical analyses however.

References

1. M. Born and E. Wolf, *Principles of Optics* (Cambridge University Press, Cambridge, 2002).
2. R.K. Luneberg, *Mathematical Theory of Optics* (University of California Press, Berkeley & Los Angeles, 1966).
3. C.L. Brockman and N.G. Alexopoulos, "Geometrical optics of inhomogeneous particles: glory ray and the rainbow revisited," *Appl. Opt.* **16**, 166-174 (1977).

4. P. Debye, "Das elektromagnetische Feld um einen Zylinder und die Theorie des Regenbogens", *Physikalische Zeitschrift* **9**, 775-778 (1908).
5. C.L. Adler, J.A. Lock, I.P. Rafferty and W. Hickok, "Twin-rainbow metrology. I. Measurement of the thickness of a thin liquid film draining under gravity," *Appl. Opt.* **42**, 6584-6594 (2003).
6. C.W. Chan and W.K. Lee, "Measurement of a liquid refractive index by using high-order rainbows," *J. Opt. Soc. Am. B* **13**, 532-535 (1996).
7. H. Hattori, H. Yamanaka, H. Kurniawan, S. Yokoi and K. Kagawa, "Using minimum deviation of a secondary rainbow and its application to water analysis in a high-precision refractive-index comparator for liquids," *Appl. Opt.* **36**, 5552-5556 (1997)
8. H. Hattori, K. Kakui, H. Kurniawan, and K. Kagawa, "Liquid refractometry by the rainbow method," *Appl. Opt.* **37**, 4123-4129 (1998).
9. H. Hattori, "Simulation study on refractometry by the rainbow method," *Appl. Opt.* **38**, 4037-4046 (1999).
10. J. Hom and N. Chigier, "Rainbow refractometry: simultaneous measurement of temperature, refractive index and size of droplets," *Appl. Opt.* **41**, 1899-1907 (2002).
11. C.L. Adler, J. A. Lock and B.R. Stone, "Rainbow scattering by a cylinder with a nearly elliptical cross section," *Appl. Opt.* **37**, 1540-1550 (1998).
12. C.L. Adler, J. A. Lock, D. Phipps, K. Saunders and J. Nash, "Supernumerary spacings of rainbows produced by an elliptical cross-section cylinder. II: Experiment," *Appl. Opt.* **40**, 2535-2545 (2001).
13. P. Massoli, "Rainbow refractometry applied to radially inhomogeneous spheres: the critical case of evaporating droplets," *Appl. Opt.* **37**, 3227-3235 (1998).

14. M. Schneider and E. D. Hirleman, "Influence of internal refractive index gradients on size measurements of spherically symmetric particles by phase Doppler anemometry," *Appl. Opt.* **33**, 2379-2388 (1994).
15. M. Schneider, E. D. Hirleman, H. Salaheen, D.Q. Choudury and S.C. Hill, "Rainbows and radially inhomogeneous droplets," in *Proceedings of the Third International Congress on Optical Particle Sizing*, M. Maeda, ed., 323-326, Yokohama, Japan, 1993.
16. P. Massoli, "Temperature and size of droplets inferred by light scattering methods: a theoretical analysis of the influence of internal inhomogeneities," presented at the 13th Annual Conference on Liquid Atomization and Spray Systems ILASS- Europe, Florence, Italy, 1997.
17. L. Kai, P. Massoli and A. D'Alessio, "Some far-field scattering characteristics of radially inhomogeneous particles," *Part. Part. Syst. Charact.* **11**, 385-390 (1994).
18. P.L. Marston, "Rainbow phenomena and the detection of non-sphericity in drops," *Appl. Opt.* **19**, 680-685 (1980).
19. J.P.A.J. van Beeck and M.L. Riethmuller, "Rainbow phenomena applied to the measurement of droplet size and velocity and to the detection of nonsphericity," *Appl. Opt.* **35**, 2259-2266 (1996).
20. J.P.A.J. van Beeck and M.L. Riethmuller, "Nonintrusive measurements of temperature and size of single falling raindrops," *Appl. Opt.* **34**, 1633-1639 (1995).
21. K. Anders, N. Roth and A. Frohn, "Influence of refractive index gradients within droplets on rainbow position and implications for rainbow refractometry," *Part. Part. Syst. Charact.* **13**, 125-129 (1996).

22. N. Roth, K. Anders and A. Frohn, "Size insensitive rainbow refractometry: theoretical aspects", presented at the Eighth International Symposium on Applications of Laser Techniques to Fluid Mechanics, Lisbon, Portugal, 1996.
23. J.W.Y. Lit, "Radius of uncladded optical fiber from back-scattered radiation pattern," *J. Opt. Soc. Am.* **65**, 1311-1315 (1975).
24. D. Marcuse, "Light scattered from unclad fibers: ray theory," *Appl. Opt.* **14**, 1528-1532 (1975).
25. H. M. Presby, "Refractive index and diameter measurements of unclad optical fibers," *J. Opt. Soc. Am.* **64**, 280-284 (1974).
26. M.R. Vetrano, J.P.A.J. van Beeck and M.L. Riethmuller, "Generalization of the rainbow Airy theory to nonuniform spheres," *Opt. Lett.* **30**, 658-660 (2005).
27. M.R. Vetrano, J.P.A.J. van Beeck and M.L. Riethmuller, "Assessment of refractive index gradients by standard rainbow thermometry," *Appl. Opt.* **44**, 7275-7281 (2005).

List of captions

Fig. 1 (a) The ray path for a single internal reflection; any point on the path is identified by its polar coordinates (ξ, θ) .

Fig. 1 (b) The geometry for the derivation of equation (10).

Fig. 2 $F(i)$ defined by equation (18a) is the incident angular component of the additional deviation incurred for the inhomogeneous sphere over that for the homogeneous one (see equation (18)), and is plotted for $n_0 = 5/3$. $F1(i)$ is for $n_0 = 2.5$.

Fig. 3 Graphs of (i) the exact ray deviation TotD(i) found from equation (10) for the profile $\bar{n}(\lambda) = (a\lambda + b)^{-1}$ with $a = \varepsilon$ ($= 0.25$ here) and $n_0 = 5/3$, corresponding to $n_1 = 5/(5\varepsilon + 3)$; (ii) the deviation for the homogeneous sphere Dh(i) for $\bar{n}(\lambda) = n_0 = 5/3$; (iii) the additional deviation $\varepsilon F(i)$, due to the inhomogeneity (see equations (18) and (18a)); (iv) the linear approximation to the deviation Dh(i) + $\varepsilon F(i)$, as calculated from equation (18).

Fig. 4 Graphs of symmetric refractive index profiles.

Fig. 5 Graphs of $D(i)$ for two symmetric refractive index profiles $\rho_1(\lambda)$ and $\rho_2(\lambda)$.]

Fig. 6 (a) Variation of refractive index $n(\lambda)$ as a function of the normalized radius λ of the sphere.

Fig. 6 (b) Variation of singular point $\rho(\lambda)$ as a function of the normalized radius λ of the sphere.

Fig. 7. Graph of $D(i)$ for $\bar{n}(\lambda) = [5 + \sin(6\pi\lambda)]/3$. Note the multiple extrema and also the apparent singular behavior near $i \approx \arcsin 0.76 = 49.5^\circ$, corresponding to the smallest minimum of $\rho(\lambda)$ in Fig. 6.

Fig. 8 Graphs of (i) $D(i)$ as given by equation (10); (ii) the integral term $L(i)$ as defined by equation (24) and (iii) the linear part of $D(i)$, namely $DI(i) = 2i$, where $D(i) = DI(i) + 4L(i) - \pi$.

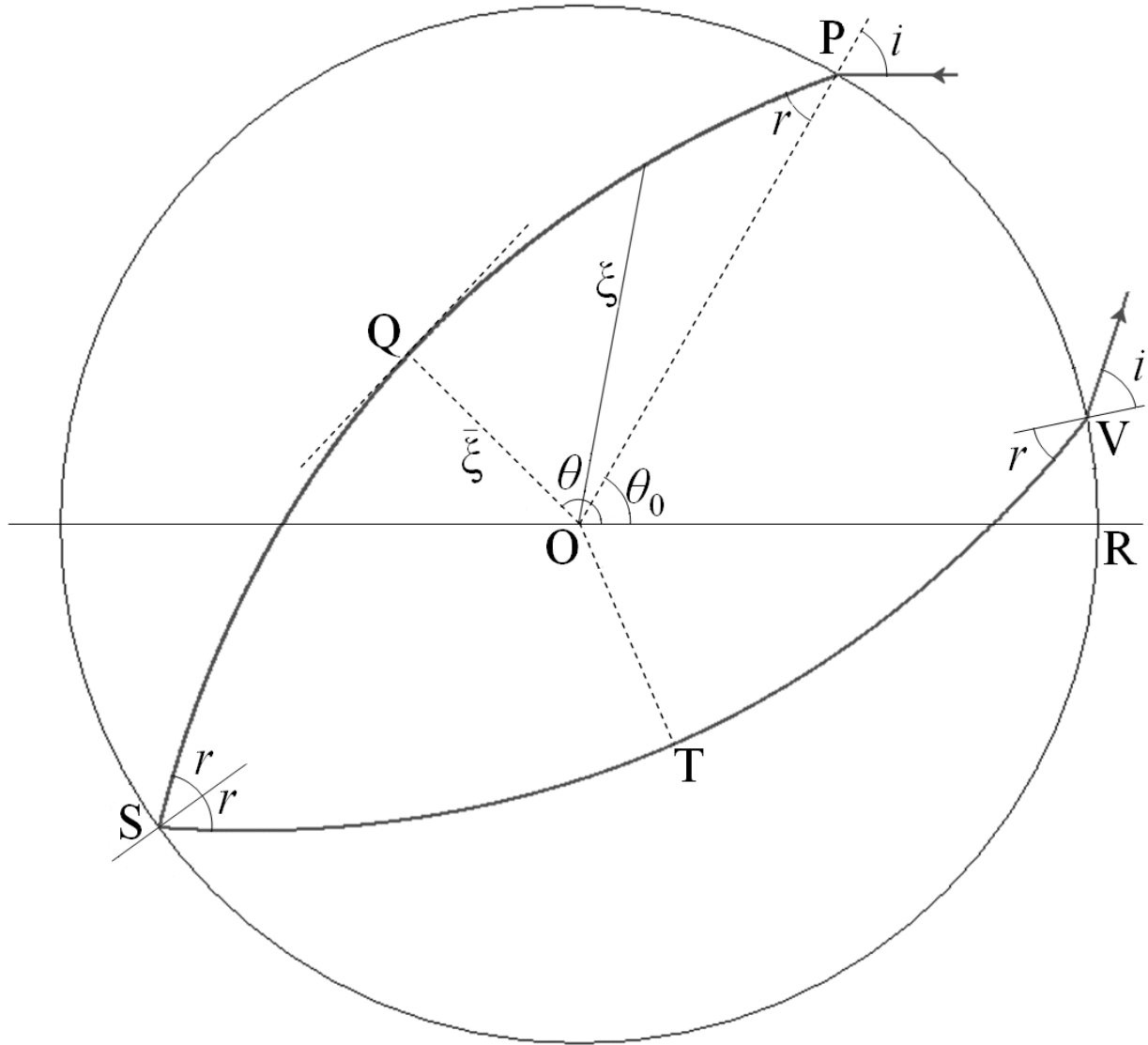


Fig. 1 (a) The ray path for a single internal reflection; any point on the path is identified by its polar coordinates (ξ, θ) .

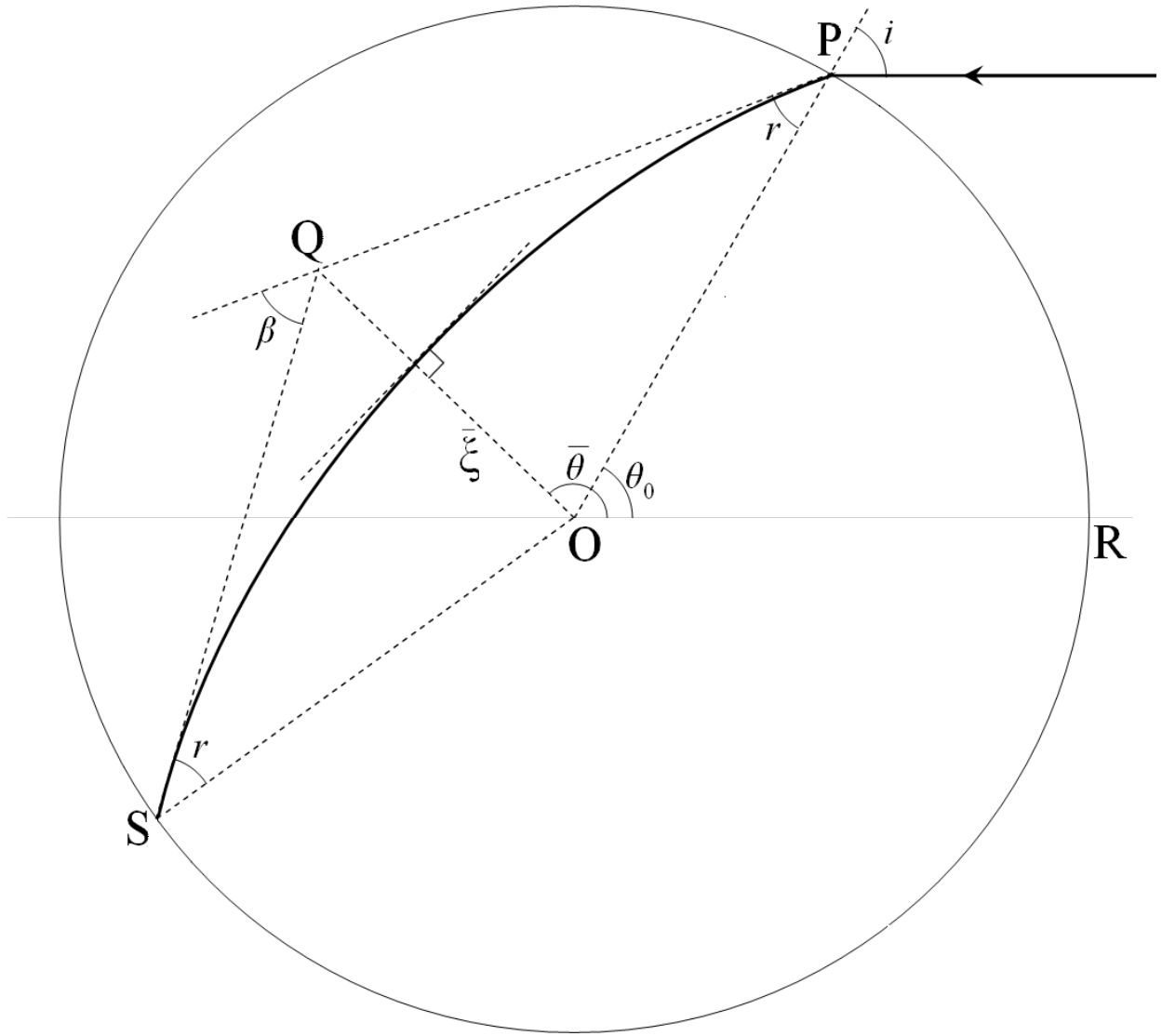


Fig. 1 (b) The geometry for the derivation of equation (10).

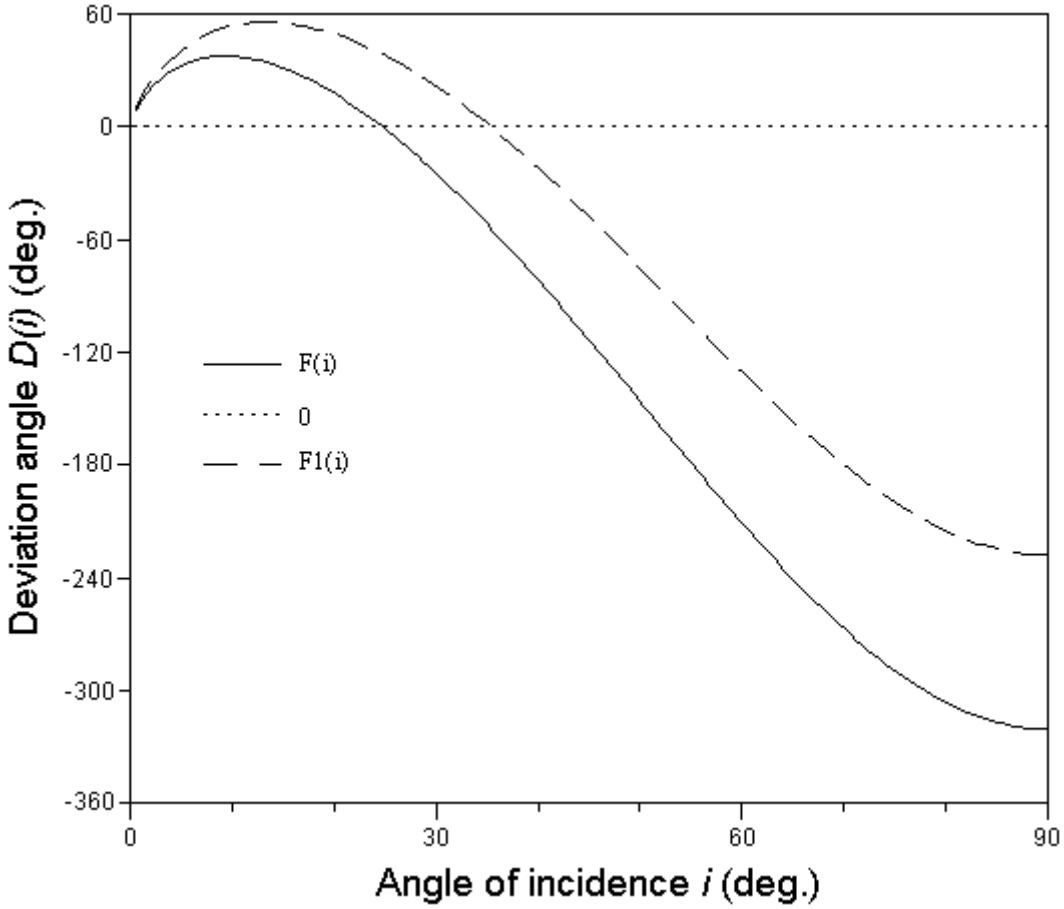


Fig. 2 $F(i)$ defined by equation (18a) is the incident angular component of the additional deviation incurred for the inhomogeneous sphere over that for the homogeneous one (see equation (18)), and is plotted for $n_0 = 5/3$. $F1(i)$ is for $n_0 = 2.5$.

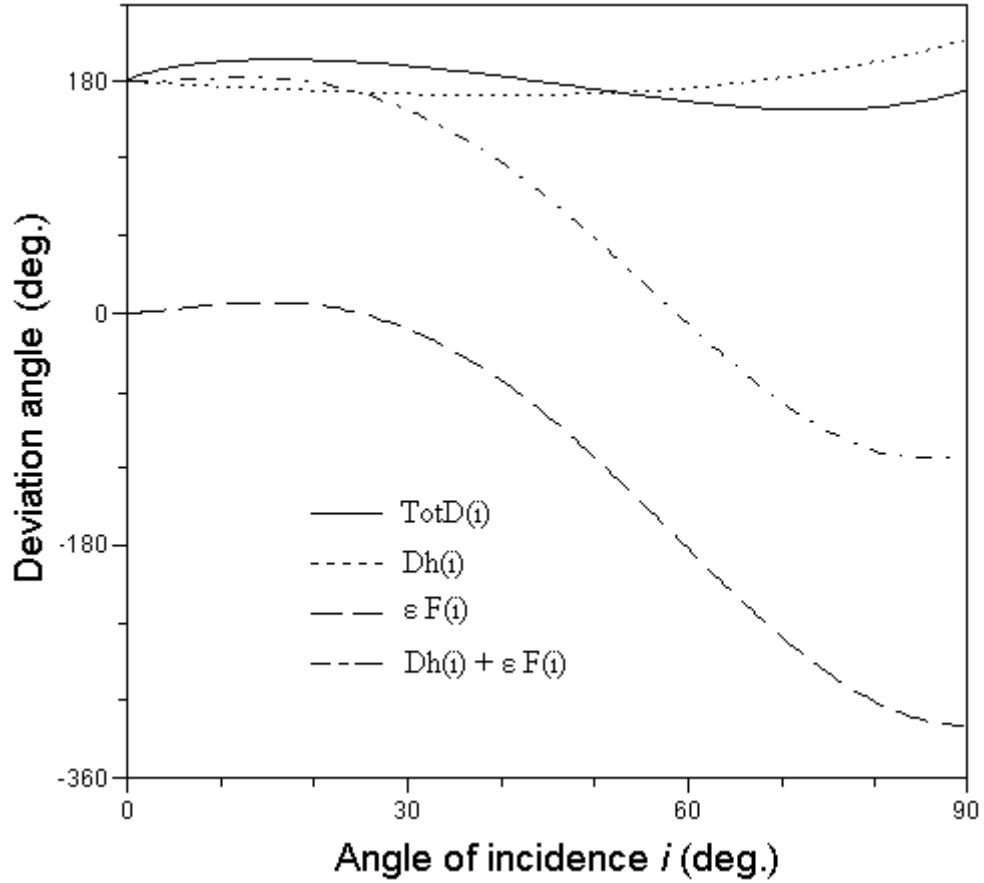


Fig. 3 Graphs of (i) the exact ray deviation $TotD(i)$ found from equation (10) for the profile $\bar{n}(\lambda) = (a\lambda + b)^{-1}$ with $a = \varepsilon$ ($= 0.25$ here) and $n_0 = 5/3$, corresponding to $n_1 = 5/(5\varepsilon + 3)$; (ii) the deviation for the homogeneous sphere $Dh(i)$ for $\bar{n}(\lambda) = n_0 = 5/3$; (iii) the additional deviation $\varepsilon F(i)$, due to the inhomogeneity (see equations (18) and (18a)); (iv) the linear approximation to the deviation $Dh(i) + \varepsilon F(i)$, as calculated from equation (18).

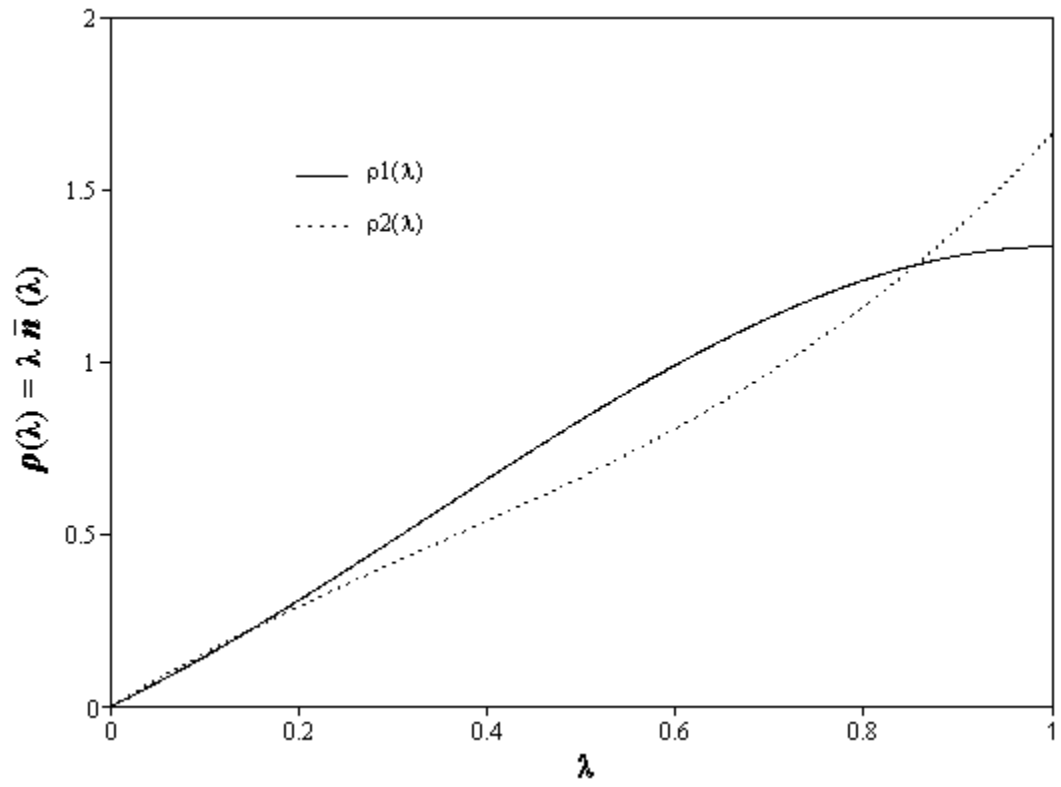


Fig. 4 Graphs of symmetric refractive index profiles.

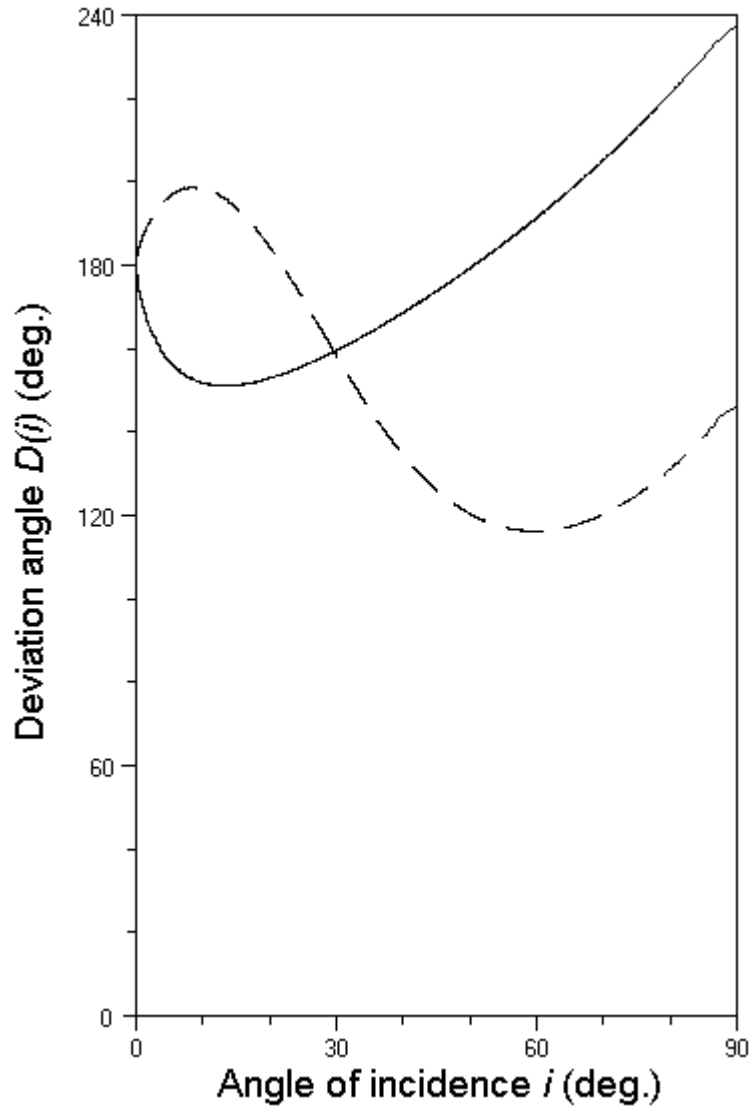


Fig. 5 Graphs of $D(i)$ for two symmetric refractive index profiles $\rho_1(\lambda)$ and $\rho_2(\lambda)$.]

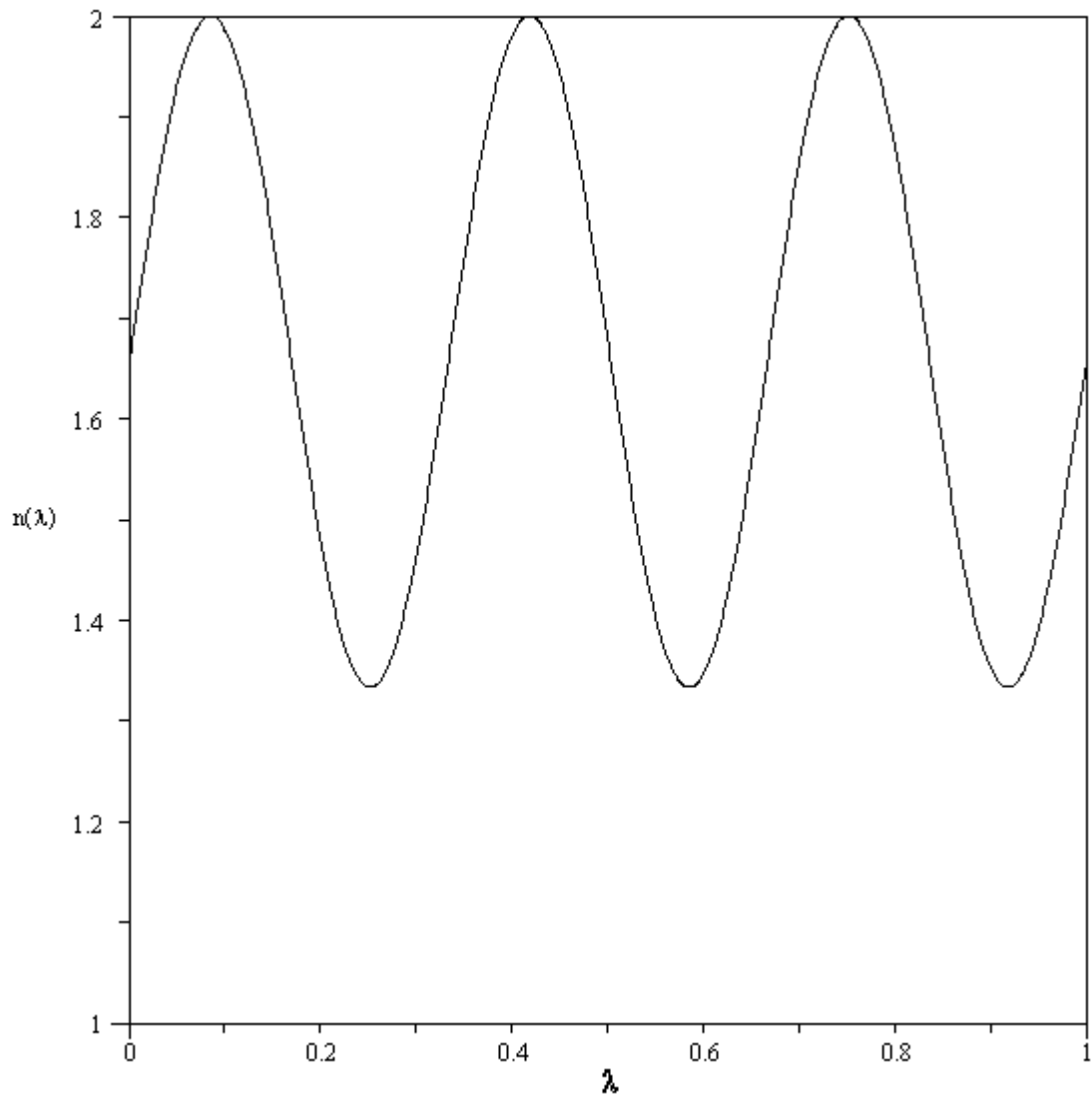


Fig. 6 (a) Variation of refractive index $n(\lambda)$ as a function of the normalized radius λ of the sphere.

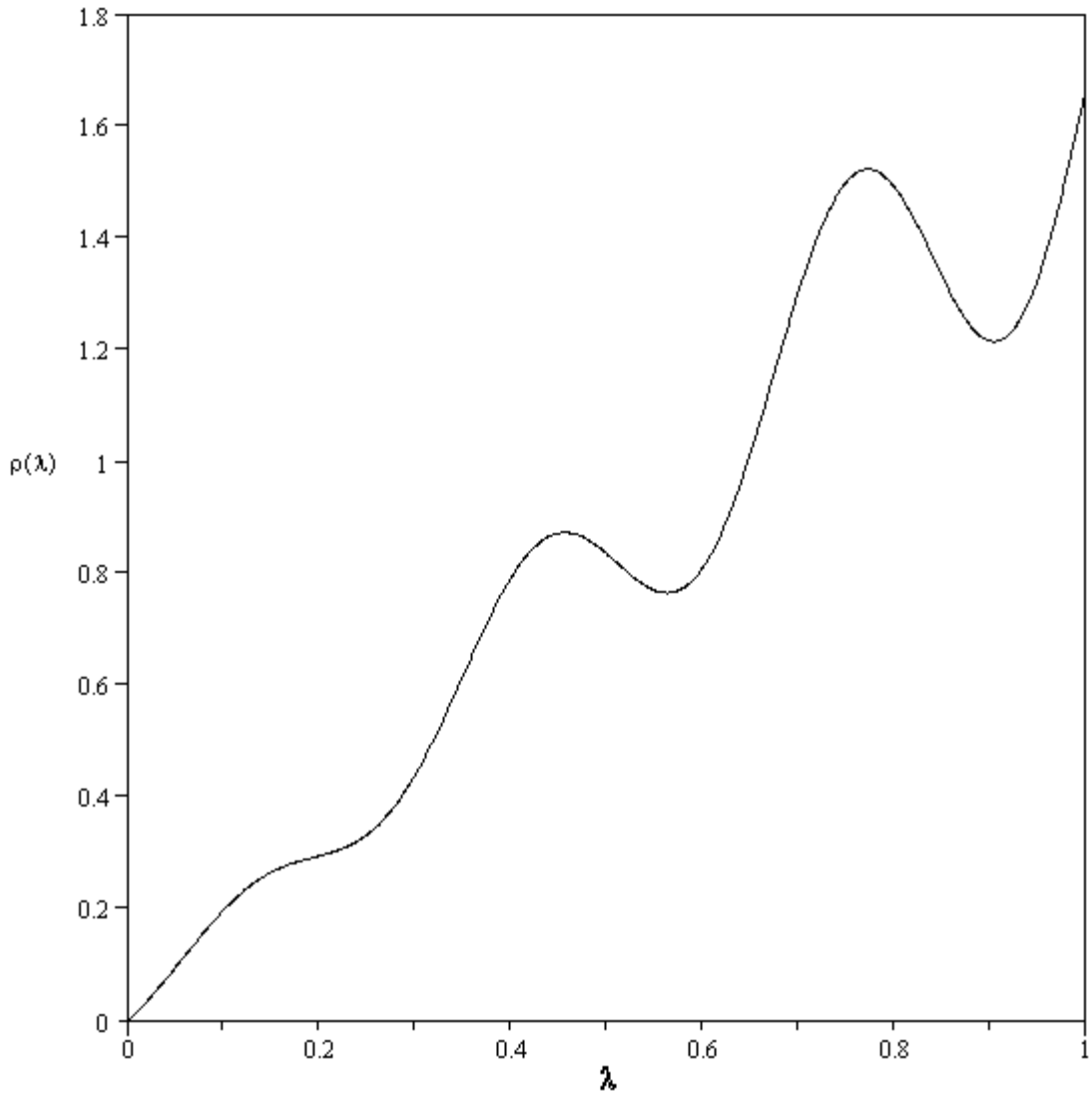


Fig. 6 (b) Variation of singular point $\rho(\lambda)$ as a function of the normalized radius λ of the sphere.

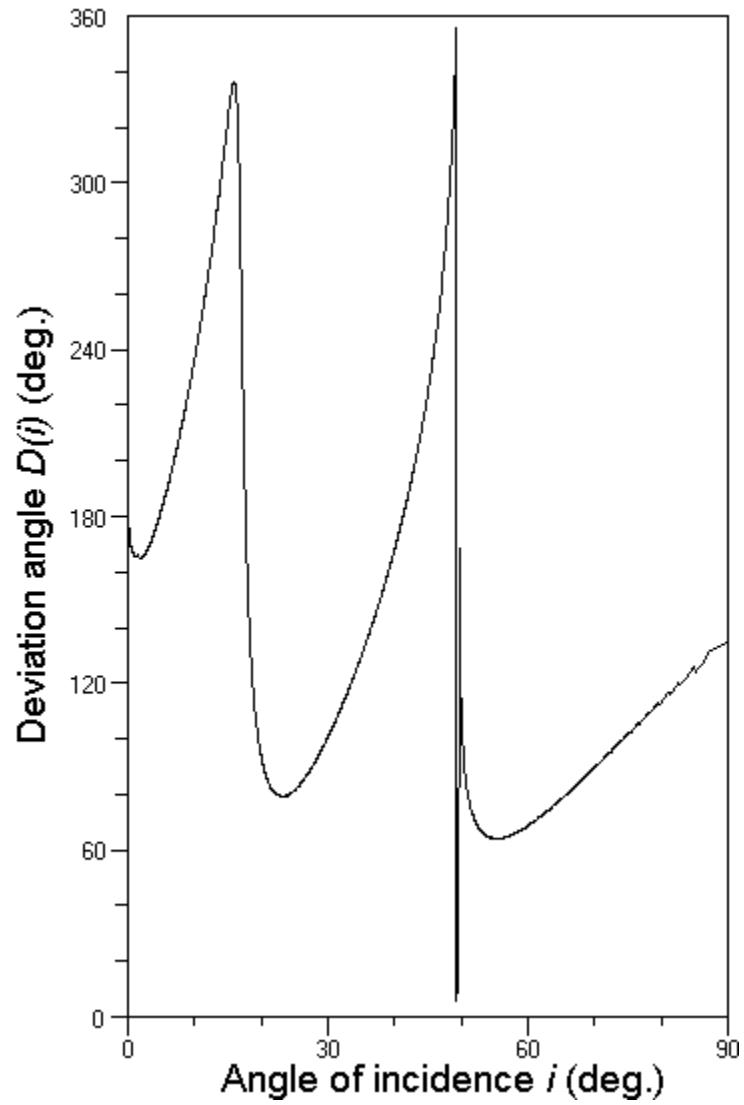


Fig. 7. Graph of $D(i)$ for $\bar{n}(\lambda) = [5 + \sin(6\pi\lambda)]/3$. Note the multiple extrema and also the apparent singular behavior near $i \approx \arcsin 0.76 = 49.5^\circ$, corresponding to the smallest minimum of $\rho(\lambda)$ in Fig. 6.

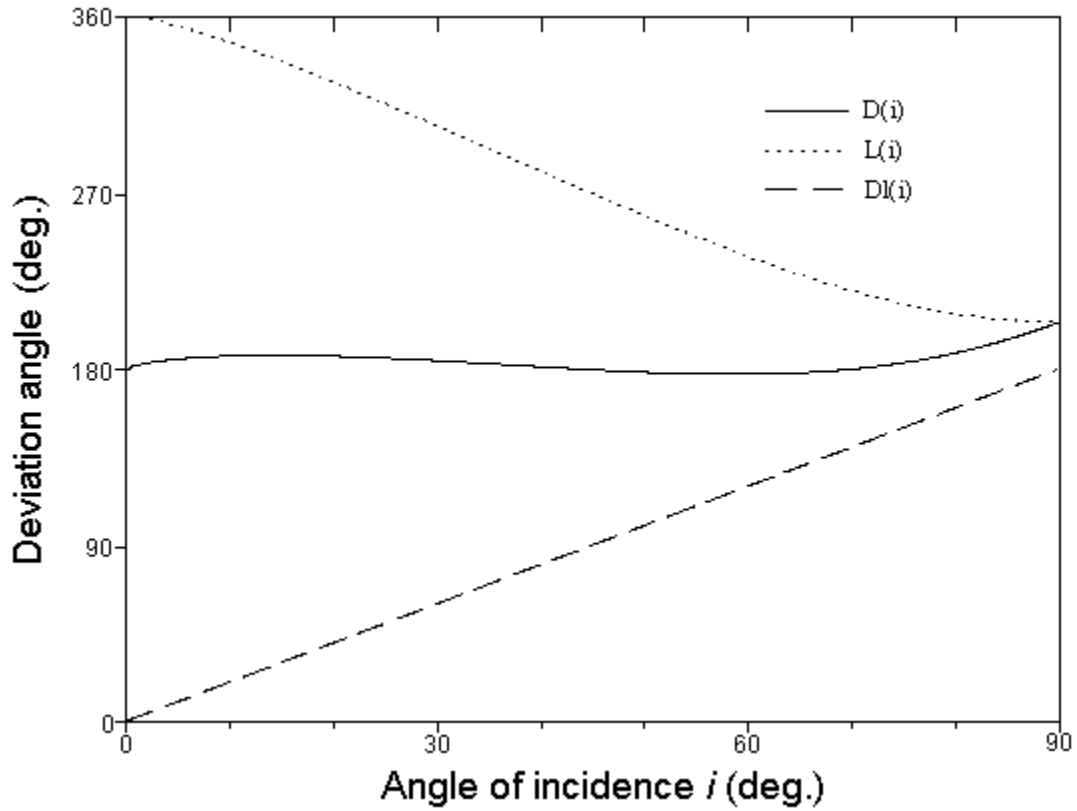


Fig. 8 Graphs of (i) $D(i)$ as given by equation (10); (ii) the integral term $L(i)$ as defined by equation (24) and (iii) the linear part of $D(i)$, namely $Dl(i) = 2i$, where $D(i) = Dl(i) + 4L(i) - \pi$.